The RNA binding protein IMP2 drives a stromal-Th17 cell circuit in autoimmune neuroinflammation

Rami Bechara [1,2 *], Nilesh Amatya [2], Saikat Majumder [2], Chunsheng Zhou[2], Yang Li[2], Qixing Liu[2,3], Mandy J. McGeachy [2] and Sarah L. Gaffen [2*]

[1] Université Paris-Saclay, CEA, INSERM UMR 1184, Centre de Recherche en Immunologie des Infections Virales et des Maladies Auto-Immunes, Le Kremlin Bicêtre, France

[2] Division of Rheumatology & Clinical Immunology, University of Pittsburgh, Pittsburgh, PA, USA

[3] Tsinghua University, Beijing, PR China

Short title: Ccl2 mRNA regulation by IMP2 underlies EAE pathogenesis

[*] Co-corresponding authors:

Sarah L. Gaffen
Department of Medicine
University of Pittsburgh
200 Lothrop Street
Pittsburgh, PA 15261
Phone: 412-383-8903
Email: sarah.gaffen@pitt.edu

Rami Bechara
INSERM UMR 1184, CEA
Faculté de Médecine
Université Paris-Saclay
Le kremlin Bicêtre, France 94270.
Phone: 33-6-51766716
Email:rami.bechara@universite-paris-saclay.fr

Conflict of interest statement: SLG has consulted for Eli Lilly and Aclaris Therapeutics. The authors declare no other competing interests.

Abstract

Stromal cells are emerging as key drivers of autoimmunity, in part by producing inflammatory chemokines that orchestrate inflammation. Chemokine expression is regulated transcriptionally but also through post-transcriptional mechanisms, the specific drivers of which are still incompletely defined. CCL2 (MCP1) is a multifunctional chemokine that drives myeloid cell recruitment. During experimental autoimmune encephalomyelitis (EAE), an IL-17-driven model of multiple sclerosis, CCL2 produced by lymph node (LN) stromal cells is essential for immunopathology. Here, we show that *Ccl2* mRNA upregulation in human stromal fibroblasts in response to IL-17 requires the RNA binding protein (RBP) insulin like growth factor 2 mRNA binding protein 2 (IGF2BP2, IMP2), which is expressed almost exclusively in non-hematopoietic cells. IMP2 binds directly to *CCL2* mRNA, markedly extending its transcript half-life and thus required for efficient CCL2 secretion. Consistent with this, *Imp2*$^{-/-}$ mice showed reduced CCL2 production in LN during EAE, causing impairments in monocyte recruitment and Th17 cell polarization. *Imp2*$^{-/-}$ mice were fully protected from CNS inflammation. Moreover, deletion of IMP2 after EAE onset was sufficient to mitigate disease severity. These data show that posttranscriptional control of *Ccl2* in stromal cells by IMP2 is required to permit IL-17-driven progression of EAE pathogenesis.

Introduction

Autoimmune diseases encompass a spectrum of disorders characterized by aberrant immunes response to self-antigens, usually of unknown etiology. Despite substantial advances in anti-cytokine biologic drugs, there is a major unmet need for more effective treatments for autoimmune conditions. Achieving this goal will require a better understanding of the molecular pathways and mechanisms that promote autoimmunity.

Multiple sclerosis (MS) is a T cell-mediated demyelinating condition of the central nervous system (CNS). Experimental autoimmune encephalomyelitis (EAE) is a widely used mouse model that has shaped our understanding of the pathogenesis of MS and many other autoimmune conditions. This model has been the impetus for effective therapeutic approaches for MS, particularly the discovery of the Th17 pathway and inhibitors thereof (1). During EAE, the generation of encephalitogenic Th17 cells is dependent on myelin antigen processing and presentation.

The chemokine ligand 2 (CCL2, MCP1) is a key player in driving EAE pathogenesis (2, 3). Deletion of *Ccl2* or its receptor CCR2 led to reduced CNS inflammation in EAE (4-7). In addition to governing leukocyte movement, CCL2 has been suggested to directly regulate T-cell priming and polarization in draining LN (2, 8). Indeed, crosstalk between stromal cells and lymphocytes is becoming increasingly appreciated, and in EAE LN stromal cells express high levels of CCL2 and actively mediate immune responses (9). Hence, CCL2 acts to trigger chemotaxis and may also sustain T cell differentiation and effector functions.

At homeostasis, the *Ccl2* gene is transcribed at low tonic levels, but is rapidly induced following exposure to inflammatory stimuli, notably by the encephalogenic cytokine IL-17A (here termed IL-17) (10-12). IL-17-family cytokines comprise a structurally and biochemically distinct class of

factors with distinct signaling mechanisms compared to other inflammatory stimuli. Consequently, IL-17 driven events still poorly defined. In recent years it has become increasingly evident that IL-17 upregulates downstream target genes in large part through post-transcriptional control of mRNA, which is orchestrated by a highly complex but still poorly-understood network of RNA binding proteins (RBPs) (13). Although transcriptional induction of *Ccl2* at the level of its promoter is well defined (14), far less is known about post-transcriptional regulation mechanisms, which are essential to determine overall mRNA levels (15).

The RNA binding protein IMP2 (also known as IGF2 mRNA binding protein 2, IGF2BP2) has been implicated in control of cellular metabolism and tumor progression. However, IMP2 is not detectably highly expressed in most hematopoietic cells and accordingly until recently has been overlooked in the context of the immune system (16, 17). We recently discovered a key role for IMP2 in driving a mouse model of autoantibody-induced glomerulonephritis (AGN). In AGN, IMP2 promotes expression of CCAAT/Enhancer binding protein (C/EBP) transcription factors in the IL-17 and TNF signaling pathways and drives downstream expression of renal-damaging effector genes (18). The role of IMP2 in other autoimmune settings remains unknown.

Here, we show that IMP2 is essential for expression of CCL2 in human stromal fibroblasts, which we demonstrate in human LN stromal cells and in mouse embryonic fibroblasts (MEFs). IMP2 functions by binding directly to *Ccl2* mRNA, prolonging *Ccl2* transcript half-life and enhancing CCL2 secretion from stromal cells. During EAE, IMP2 is essential for inducible expression of CCL2 within the LN. Consequently, loss of IMP2 leads to impaired monocyte accumulation in LN and concomitantly impaired Th17 cell differentiation during EAE. Thus, *Imp2*$^{-/-}$ mice are fully resistant to EAE, indicating that control of CCL2 expression at a posttranscriptional level is required for autoimmune disease progression. Moreover, inducible loss

of IMP2 after initiation of EAE also lessens disease. Together these data indicate that IMP2 is at the nexus of a stromal cell/T cell autoimmune circuit that drives neuroinflammation through a CCL2-Th17 cell axis.

Results

Imp2-deficient mice are resistant to EAE

To interrogate a role for IMP2 in EAE, we induced disease in mice by immunization with myelin oligodendrocyte glycoprotein peptide (MOG 35-55) in CFA. Mice were scored daily for signs of ascending paralysis. *Imp2*$^{+/+}$ control mice developed a typical onset and clinical course of EAE, peaking at 14–16 days post immunization **(Figure 1A)**. As previously shown, mice lacking the IL-17 receptor (*Il17ra*$^{-/-}$) were fully resistant to signs of disease (19). Strikingly, *Imp2*$^{-/-}$ mice showed resistance to EAE that was similar to *Il17ra*$^{-/-}$ mice **(Figure 1A).** Concomitant with reduced disease scores, there was marked reduction in incidence of EAE in *Imp2*$^{-/-}$ mice **(Figure 1B)**. Thus, IMP2 is essential for autoimmune inflammation in EAE.

Disease in EAE is mediated by the accumulation of pathogenic Th17 cells in the CNS. To determine if IMP2 impacts Th17 cell infiltration during EAE, mice were immunized with MOG, and CNS tissues harvested at day 16 were stimulated with PMA/ionomycin and stained for T cell markers and intracellular cytokines. Consistent with the observed decrease in EAE severity, *Imp2*$^{-/-}$ mice presented decreased numbers of IL-17-, IFNγ- and GM-CSF-producing CD4^{+} T-cells **(Figure 1C-E; Supp figure 1)**. Together, these results indicate that IMP2 is required for pathogenic Th17 cell infiltration in CNS and thus for EAE pathogenesis.

Imp2-deficient mice showed impaired Th17 cell generation in LN

To understand the cause of decreased encephalitogenic Th17 cell frequencies in the setting of IMP2 deficiency, we assessed T cell differentiation in *Imp2*$^{-/-}$ mice. Mice were immunized with MOG and draining (inguinal) LN were harvested at day 10, stimulated with PMA/ionomycin and stained for T cell markers and intracellular cytokines **(Supp figure 2)**. Both the percentages and

total numbers of IL-17-producing T cells were reduced in *Imp2*$^{-/-}$ compared to *Imp2*$^{+/+}$ littermates **(Figure 2A)**. In contrast, IMP2 did not impact IFNγ or IL-10 production **(Figure 2B, C)** or LN infiltration of total CD4^{+} cells **(Supp figure 2A)**. There were no baseline differences in expression of T cell cytokines in naïve mice of both genotypes **(Supp figure 3).**

IMP2 drives Ccl2 expression and monocyte recruitment in LN

IL-17 triggers potent downstream signaling activities on LN stromal cells (20, 21). To delineate the impact of IMP2 on LN during EAE, *Imp2*$^{+/+}$ and *Imp2*$^{-/-}$ LNs were subjected to RNAseq at day 7 post-EAE. A total of 383 genes were differentially regulated, and Ingenuity Pathway Analysis (IPA) identified multiple differentially enriched pathways. Notably, hypercytokinemia and hyperchemokinemia were among the most altered pathways in *Imp2*$^{-/-}$ mice **(Figure 3A)**. Prominent among differentially expressed genes was CCL2, which is known to promote EAE by enhancing monocyte recruitment. CCL2 has also been described to promote Th17 cell polarization directly (4-8). *Imp2*$^{-/-}$ mice showed significantly decreased expression in *Ccl2* mRNA in LN on day 7 post-EAE **(Figure 3B)**. Although *Ccl2* was upregulated in spinal cords of mice with EAE, its expression was not statistically reduced in *Imp2*$^{-/-}$ mice (**Figure 3C**). The major CCL2-expressing cells in LN are in the non-hematopoietic (CD45^{-}) stromal compartment (9), cells that are known to be responsive to IL-17 (20). To determine if IMP2 in LN stromal cells is required to upregulate *Ccl2*, CD45^{-} populations isolated from LN of *Imp2*$^{+/+}$ and *Imp2*$^{-/-}$ naïve mice were treated with IL-17 for 24 hours, and CCL2 in supernatants was assessed by ELISA. CCL2 levels were elevated after IL-17 stimulation in the CD45^{-} fraction in *Imp2*$^{+/+}$ but were impaired *Imp2*$^{-/-}$ cells **(Figure 3D)**. CCL2 was not detectable in the CD45^{+} fraction (data not shown). Together, these data suggest a stromal-intrinsic role of IMP2 in driving CCL2 expression in response to IL-

17.

A major function of CCL2 is to recruit monocytes to sites of inflammation. Indeed, IMP2 was required for monocyte accumulation in LN during EAE, with *Imp2*$^{-/-}$ mice showing reduced accumulation of CD45^{+}Ly6C^{+}Ly6G^{-} monocytes compared to *Imp2*$^{+/+}$ controls **(Figure 3E)**. In contrast to monocytes, *Imp2*$^{+/+}$ and *Imp2*$^{-/-}$ mice showed similar infiltration of other myeloid cell populations during EAE, demonstrating an especially key activity of monocyte-recruiting chemoattractants such as CCL2 **(Supp figure 4).**

According to ImmGen, IMP2 is expressed at extremely low levels in most immune cells. Indeed, IMP2 was not detectable in CD4^{+} T cells either in Th0 or Th17 conditions **(Figure 4A)**. To determine if there is a T cell-intrinsic role for IMP2 in Th17 or Th1 differentiation, naïve CD4^{+} T cells from *Imp2*$^{+/+}$ and *Imp2*$^{-/-}$ mice were stimulated for 3 days with plate bound anti-CD3 and anti-CD28 under Th0 or standard Th17 conditions (IL-6, TGF-β, IL-1β and IL-23) or Th1 conditions (IL-12) **(Figure 4B)**. As shown, *Imp2* deficiency did not impact percentages of in vitro-generated CD4^{+}IL-17^{+} Th17 cells, IL-17 production, or *Il17a* and *Rorc* expression **(Figure 4C-E)**. Similarly, IMP2 did not affect Th1 differentiation **(Figure 4F)**. Thus, T cells from *Imp2*$^{-/-}$ mice are not inherently defective in the ability to differentiate to the Th17 or Th1 lineage, at least when using optimal polarizing cytokine conditions **(Figure 4B)**.

In addition to governing leukocyte movement, CCL2 was reported to promote development of polarized Th17 responses, and CCR2 deficiency in T cells caused decreased Th17 cell frequencies in vivo (8). However, we found that adding CCL2 to the optimal or suboptimal Th17 polarizing conditions did not impact IL-17 production **(Figure 4G, H)**. Interestingly, in suboptimal conditions there was a modest but significant decrease in IL-17 production in *Imp2*$^{-/-}$ CD4^{+} T cells,

suggesting there may be subtle T cell-intrinsic capabilities of this RBP, which will need further investigation **(Figure 4H)**.

IMP2 mediates post-transcriptional regulation of Ccl2 mRNA

We next interrogated the role of IMP2 on IL-17 induction of CCL2 in human LN stromal cells, focusing on fibroblastic reticular cells (FRC) as these are key responders to IL-17. Primary human FRCs ($CD45^-CD31^-gp38^+$) were treated with IL-17 in the presence or absence of *IMP2* siRNA. IL-17 treatment upregulated *CCL2* in FRCs, peaking at 2 h and sustained over 24 h (**Figure 5A**). Knockdown of IMP2 efficiently abrogated IL-17-mediated upregulation of *CCL2* (**Figure 5B**). Similarly, *Imp2* silencing suppressed IL-17-mediated upregulation of *Ccl2* in primary murine fibroblasts (**Figure 5C**), and IL-17 enhanced *Ccl2* mRNA and CCL2 protein were abrogated in *Imp2*$^{-/-}$ MEFs (**Figure 5D-F**). IMP2 also regulated *Ccl2* mRNA and protein in response to TNFα, IL-17F as well as IL-1β **(Figure 5G, H)**. Thus, IMP2 is required for cytokine-induced upregulation of CCL2 in primary mouse and human fibroblasts.

IMP2 is known to regulate target mRNA stability and translation, typically by binding to regulatory elements in 3' or 5'UTR motifs (22-24). Hence, we evaluated the capacity of IMP2 to bind to *Ccl2* mRNA by RNA immunoprecipitation (RIP). Cells were treated with IL-17, immunoprecipitated with anti-IMP2 Abs or control IgG, and lysates evaluated for *Ccl2* mRNA. IMP2 RIP samples were substantially enriched in *Ccl2* mRNA compared to IgG controls, demonstrating that *Ccl2* is a direct IMP2 'client' transcript (**Figure 6A)**. To determine if IMP2 interacts with the *Ccl2* 3'UTR, we co-expressed a *Ccl2*-3'UTR-Luciferase fusion construct with FLAG-tagged IMP2 in human embryonic kidney (HEK) 293 cells. Lysates were subjected to RIP with anti-FLAG Abs, and *Luc* mRNA enrichment assessed by qPCR. As shown, there was

substantial association of IMP2 with *Luc* mRNA, indicating that IMP2 can bind the *Ccl2* 3'UTR **(Figure 6B)**. To determine if IMP2 enhances *Ccl2* RNA stability, *Ccl2* mRNA half-life ($t_{½}$) was assessed using a standard actinomycin mRNA decay assay in MEFs (25-27). As shown, IL-17 promoted *Ccl2* longevity ~2-fold, increasing the $t_{½}$ from 122 m to 275 m (**Figure 6C**). In both untreated and IL-17-treated conditions, *Ccl2* mRNA had a shorter $t_{½}$ in *Imp2*$^{-/-}$ compared to *Imp2*$^{+/+}$ cells (~85 m) **(Figure 6C)**. Collectively, these data demonstrate that *Ccl2* is an IMP2 client mRNA and that IL-17 enhances *Ccl2* mRNA by promoting transcript stabilization.

We and others recently showed that IMP2 recognizes many of its client mRNAs through the N6-methyladenosine (m^{6}A) 'epitranscriptomic' RNA modification, for example *Cebpd* and *Myc* (18, 28, 29). However, *Ccl2* has very few predicted m^{6}A consensus sites based on public databases (RMBase and SRAMP). To determine empirically whether *Ccl2* contains m^{6}A modifications, we performed RIP with anti-m^{6}A Abs. As previously shown, *Cebpd* mRNA was substantially increased upon m^{6}A RIP (MeRIP), both at baseline and after IL-17 treatment (18) **(Figure 6D)**. *Ccl2* was also detected in MeRIP samples but at a much lower level than *Cebpd*, which is commensurate with its limited number of predicted m^{6}A motifs **(Figure 6D)**.

The RBP Hu-antigen R (HuR) has been implicated in regulating inflammatory mRNAs including chemokines activated by IL-17 (26, 30). HuR also interacts with multiple binding partners including IMP2 that determine its target transcript specificity (28, 31). Like IMP2, knockdown of *HuR* impaired expression of *Ccl2* mRNA, in agreement with prior reports (32) (**Supp Figure 5A**). In addition, knockdown of *HuR* in combination with *Imp2* reduced the expression of *Ccl2* more profoundly than knockdown of *Imp2* alone, consistent with a model in which IMP2 and HuR act cooperatively to induce *Ccl2* expression. To determine whether the interaction between IMP2 and HuR is RNA-dependent, MEF lysates were treated with RNase A

and immunoprecipitated with anti-IMP2 Abs. Although RNAse A treatment had some nonspecific effects on total IMP2 levels, there were reduced interactions between IMP2 and HuR (**Supp Figure 5B**), suggesting that RNA bridges or otherwise stabilizes HuR and IMP2 interactions.

Imp2 deletion post-EAE alleviates disease

To date, there are no available pharmacological or other clinically applicable inhibitors of IMP2. To determine if loss of IMP2 after disease initiation could ameliorate EAE, $Imp2^{fl/fl}$ mice were crossed to mice with a constitutive tamoxifen (TAM)-inducible Cre ($Rosa26^{CreERT2}$), thus permitting gene deletion only upon administration of TAM. Mice were given TAM at day 7 and 8 after induction of EAE and disease signs were scored through day 21 **(Figure 7A)**. Mice in which IMP2 was deleted after MOG immunization ($Imp2^{fl/fl}$ $Rosa26^{CreERT2+}$) showed reduced EAE clinical signs as well as delayed disease incidence **(Figure 7B)**. Consistent with this, mice also exhibited reduced numbers of Th17 cells but not Th1 cells in draining LN (**Figure 7C, D**). These data show that the effects of IMP2 on inflammation are not developmental, and that blockade of IMP2 could potentially be the basis of a therapeutic approach in autoimmune disease.

Discussion

CCL2 is best recognized for its ability to promote monocyte recruitment during host defense (33). CCL2 also drives pathogenic inflammation and has therefore been implicated in many autoinflammatory diseases including multiple sclerosis (3-6). Hence, tight regulation of CCL2 is crucial to maintain a balanced immune response that permits immunity to infection without causing autoimmune sequelae or a cytokine storm.

Here, we show that amplification of *Ccl2* is mediated by IL-17 in mesenchymal cells from both mouse as well as human LN stroma. Often, induction of inflammatory genes is viewed in the context of promoter regulation, but many immune genes including *Ccl2* are expressed at baseline tonic levels, and their capacity to be induced during immune insult is due to expanded transcript half-life or other post-transcriptional mechanisms (34). IMP2, like its binding partner HuR, promotes *Ccl2* transcript stabilization, which is ultimately required for enhanced CCL2 secretion from LN stromal cells (32, 35). In addition, IMP2 and HuR interact in an RNA-dependent manner to stabilize *Ccl2* mRNA. While IMP2 functions primarily in non-hematopoietic cells by virtue of selective expression in these cell types (18), HuR is more widely expressed and has more profound impacts on Th17 cells in addition to acting on IL-17-responsive cells (36-38). Therefore, it is likely that HuR also drives IMP2-independent roles in disease pathogenesis. Given the prominent role of CCL2 in inflammation, there are also negative regulators of *Ccl2* mRNA that offset stabilizing effects. For example, tristetraprolin (TTP, *Zfp36*) is a well-characterized zinc-finger RBP that destabilizes *Ccl2* mRNA (35). Hence, multiple RBPs converge on *Ccl2* expression control.

Most of what is known about IMP2 comes from studies of metabolism and cancer (17). As suggested by its gene name *Igf2bp2* (IGF2 mRNA binding protein 2), IMP2 promotes expression of insulin-like growth factor 2 by binding to its 5' UTR and controlling translation (39). In this

regard, altered expression of components of the IGF system have been observed in MS (40-42). However, in contrast to IMP2, IGF2 alleviates EAE pathogenesis, and mice treated with IGF2 neutralizing antibodies showed increased EAE disease severity (43).

Mice lacking IMP2 are less susceptible to an autoantibody-induced glomerulonephritis (AGN) driven by IL-17 regulation of C/EBPs transcription factors, specifically in the non-hematopoietic compartment (18). Although C/EBPs are implicated in CCL2 regulation, their expression in LN and spinal cords of *Imp2*$^{-/-}$ mice is not altered. Indeed, C/EBP expression in myeloid cell lineage is most likely implicated in EAE pathogenesis (44) rather than its expression in the stromal compartment where IMP2 is mostly expressed. We and others recently showed that IMP2 recognizes many of its client mRNAs through m^{6}A RNA modification (18, 28). However, according to public databases *Ccl2* has only a few predicted m^{6}A consensus sites within its 3' UTR (45, 46), and results from our m^{6}A RIP pulldowns showed only modest enrichment of *Ccl2* mRNA. Interestingly, a recent report indicates that *Ccl2* mRNA stability can also be negatively regulated by m^{6}A through binding of the destabilizing protein TTP and the m^{6}A reader YTHDF2. Moreover, TTP promoted global increases in m^{6}A methylation through upregulation of the methylation machinery (47). Therefore, the impact of this RNA modification can be both positive and negative depending on context.

Although *Ccl2* was upregulated in the CNS of *Imp2*$^{+/+}$ mice during EAE, its expression was not statistically reduced in *Imp2*$^{-/-}$ CNS. This result suggests that IMP2 may exert distinct effects in different tissues. Moreover, IMP2 is enriched in CNS and is required for axon pathfinding and neurogenesis after hypoxic-ischemic brain injury (48-50). Even so, since loss of IMP2 after onset of EAE alleviates disease, it is unlikely that these developmental activities are needed for autoimmune pathogenesis. Ultimately, tissue-specific deletions of IMP2 will be needed to dissect

its roles in given cell types relevant to EAE.

The vital role of fibroblasts in controlling inflammation during autoimmunity has become increasingly appreciated (51, 52). Our finding that LN stromal cells express high levels of CCL2 agrees with work showing that non-hematopoietic stromal cells in LN, especially fibroblastic reticular cells (FRCs), serve as the major source of CCL2 following immunization-induced inflammation (9). Like CCL2, IMP2 is expressed almost exclusively in non-hematopoietic cells, which is in concordance with its role in regulating *Ccl2* expression. Similarly, IL-17 signaling occurs predominantly in non-hematopoietic cell types (13). Moreover, in EAE, IL-17 drives metabolic reprogramming to support proliferation of FRC during LN expansion, as well as enhancing expression of inflammatory cytokines (20).

Beyond their well-established role in providing structural support to organs, stromal and mesenchymal cells are actively involved in immune responses. FRCs in lymphoid organs regulate adaptive immunity, mesenchymal cells in adipose tissue promote Treg cell differentiation, and stromal cells in the synovium are key determinants of the inflammatory response during arthritis (20, 51, 53-55) . CCL2 was reported to modulate Th17 cell differentiation directly (8), but we observed no impact of CCL2 on promoting Th17 polarization, regardless of differentiation conditions employed. Although there was no detectable effect of IMP2 on Th17 polarization under standard differentiation conditions, IL-17 production was lower in *Imp2*-deficient T cells when cultured in suboptimal differentiation conditions, though the basis for this remains unknown. Therefore, we posit that IMP2 orchestrates a feed-forward amplification loop that sustains Th17 generation primarily by stabilizing *Ccl2* mRNA in stromal cells and promoting monocyte recruitment, and to a much lesser extent by acting directly on T cells to promote Th17 differentiation.

In summary, we have uncovered a pathway that dictates post-transcriptional regulation of *Ccl2* mRNA occurring within LN stromal cells and mediated by IL-17. The resulting increase in CCL2 leads to enhanced monocyte recruitment and Th17 cell activation, which is the basis for inflammatory pathogenesis mediated by IL-17. Therapeutic IL-17 blockade is highly effective in psoriasis and psoriatic arthritis and is being explored in other conditions (19). Preliminary trials of anti-IL-17A biologics in MS have shown some promising hints of efficacy (56, 57), though this cytokine is certainly not the sole factor driving pathogenesis (58). Strikingly, deletion of IMP2 after EAE onset ameliorated signs of disease, suggesting that IMP2 could be a viable pharmacological target. RNA-based therapeutic approaches are gaining momentum, as they can potentially be highly specific and act on conventionally un-druggable targets (59). Hence, understanding the molecular players involved in RNA regulation may ultimately offer new therapeutic avenues.

Methods

Study design

The objective of this study was to determine how CCL2 is regulated in response to IL-17. We used cell culture studies and EAE mouse model to define the role of IMP2 in IL-17-induced CCL2 production. Sample sizes were determined by power analyses from pilot or previously published data. Experiments were done 2-3 independent times. Data from multiple experiments were pooled unless noted.

Mice

All mice were on the C57BL/6 background. Cohorts were age (8-12 weeks) and sex-matched. *Imp2*$^{-/-}$ mice were from Oxford, UK. WT controls were generated in house by breeding. *Imp2*$^{fl/f}$ and *Rosa26*^{ERT2} mice were from The Jackson Laboratory (Bar Harbor, ME). *Il17ra*$^{-/-}$ mice were kindly provided by Amgen (Thousand Oaks, CA). Mice were housed in SPF conditions. Protocols were approved by the University of Pittsburgh IACUC.

EAE

Mice were immunized subcutaneously in 2 sites on the back with 100 μg MOG peptide (35–55) (Biosynthesis) emulsified with Complete Freund's Adjuvant (CFA) with M. tuberculosis strain H37Ra (DIFCO Laboratories). Mice also received 100 ng pertussis toxin (List Biological Laboratories) i.p. on day 0 and day 2. Mice were assessed daily and scored as follows: 1, flaccid tail; 2, impaired righting reflex and hindlimb weakness; 3, partial hindlimb paralysis; 4, complete hindlimb paralysis; 5, hindlimb paralysis with partial forelimb paralysis; 6, moribund. For *Imp2*

inducible deletion, mice were administered tamoxifen (2 mg, i.p) on day 7 and 8 post-EAE induction.

Cell Culture and cytokine stimulation

MEFs cells (made from C57BL/6J or *Imp2*$^{-/-}$ mice, both male and female) were cultured in α-minimum essential medium (α-MEM; Sigma-Aldrich, St. Louis MO) with L-glutamine, antibiotics and 15% FBS. Human stromal cells were cultured in RPMI (α-MEM; Sigma-Aldrich, St. Louis MO), with L-glutamine, antibiotics and 10% FBS. IL-17A and IL-17F (PeproTech, Rocky Hill, NJ) were used at 200 ng/ml. TNFα and IL1β (PeproTech) were used at 10 ng/ml. Actinomycin D (Sigma-Aldrich) was used at 10 μg/ml.

Human FRCs

Human tonsils from sleep apnea patients were incubated in digestion medium (RPMI, 0.1 mg/ml DNase I (Invitrogen) and 0.2 mg/ml liberase (Roche). Single-cell suspensions were filtered and subjected to red blood cell lysis. CD45^{+} CD31^{+} cells were magnetically removed using an EasySep Human APC Positive Selection kit (Stemcell). The gp38^{+} FRC population was positively selected using an EasySep Human PE Positive Selection kit (Stemcell) and rested for 2-3 days. Purity of the FRC populations were tested by flow cytometry and were > 95%.

siRNA transfection

ON-TARGETplus SMARTpool siRNAs targeting IMP2 were from Dharmacon (Lafayette, CO). For RNA silencing, MEFs and human stromal cells were seeded overnight in antibiotic-free media.

Transfection was performed 18 h later with 50 nM siRNA in DharmaFECT Reagent 1. Culture media was replaced after 24 h, and cytokines administered 24 h later.

qPCR, RNAseq and RNA immunoprecipitation (RIP)

RNA was isolated with RNeasy Mini Kits (Qiagen). Complementary DNA was synthesized by SuperScript III First Strand Kits (Thermo Fisher Scientific, Waltham MA). Real-time qPCR was performed with SYBR Green FastMix ROX (Quanta Biosciences) on a 7300 Real-Time instrument (Applied Biosystems), normalized to *Gapdh*. Primers were from QuantiTect Primer Assays (QIAGEN).

For RNASeq, complementary DNA (cDNA) libraries were prepared from lymph nodes RNA harvested day 7 after EAE induction (Nextera XT Kit) and RNASeq was performed on the Illumina NextSeq 500 platform by the Health Sciences Sequencing Core at the University of Pittsburgh. Sequencing reads were annotated and aligned to the UCSC (University of California, Santa Cruz) mouse reference genome (mm10, GRCm38.75) using HISAT. HISAT alignment files were used to generate read counts for each gene, and determination of differential gene expression was performed using the DE-seq package from Bioconductor. Unbiased hierarchical clustering of differentially expressed genes with $P < 0.05$ was calculated using CLC Genomics Workbench. Relative expression values in heat maps are RPKM (Reads Per Kilobase Million) values per sample that have been divided by the average expression across all samples.

For IMP2 RIPs, extracts were isolated with lysis buffer [100 mM KCl, 5 mM $MgCl_2$, 10 mM HEPES (pH 7.0), 0.5% NP-40, 1 mM dithiothreitol] with RNAse Out (100 U/ml, Invitrogen). Buffers included a protease inhibitor cocktail (Sigma-Aldrich). Lysates were precleared protein A agarose (Roche Applied Science) and immunoprecipitated with Abs against IMP2 (MBL;

RN008P) or isotype control (MBL; PM035). Beads were washed with NT2 buffer and digested with DNase I (Roche Applied Science) and protease K (Sigma). Total RNA was extracted with acid phenol.

For MeRIP, 20 to 50 μg of RNA was fragmented and purified by ethanol precipitation. A total of 0.1 fmol of a control m^6A-modified Gaussia Luc RNA or unmodified Cypridina Luc RNA (supplied with the EpiMark m^6A Enrichment kit; New England Biolabs; E1610S) were spiked in each sample. For RIP, Protein G Dynabeads (Thermo Fisher Scientific) were washed in MeRIP buffer [150 mM NaCl, 10 mM tris-HCl (pH 7.5), and 0.1% NP-40] and incubated with anti-m^6A Abs for 2 h at 4°C. After washing, anti-m^6A–conjugated beads were incubated with mRNA for 4 h in RNasin (Promega). Up to 3% of mRNA was used for input. Beads were washed with MeRIP buffer, low-salt wash buffer [50 mM NaCl, 10 mM tris-HCl (pH 7.5), and 0.1% NP-40], and wash buffer [500 mM NaCl, 10 mM tris-HCl (pH 7.5), and 0.1% NP-40]. m^6A-modified RNA was eluted in MeRIP buffer containing 5 mM m^6A salt (Santa Cruz Biotechnology). Eluates were pooled and concentrated by ethanol precipitation. Input and IP fractions were reverse transcribed using the iScript cDNA synthesis kit (Bio-Rad) and subjected to qPCR

RNA decay analysis

MEFs were primed with TNFα (10 ng/ml) for 3 h. Cells were washed with PBS and treated with 10 μg/ml actinomycin D (ActD; Sigma-Aldrich) ± 200 ng/ml IL-17 as described (26). Levels of mRNA were assessed by qPCR. For each mRNA, remaining quantity (%) was calculated by normalizing ΔΔCt to the ΔΔCt of samples primed with TNFα.

In vitro T cell differentiation

Naive splenic $CD4^+$T cells were purified by magnetic separation (Miltenyi Biotec). T cells were activated with anti-CD28 (5mg/ml; Bio-XCell) and plate-bound anti-CD3 (clone 145-TC11, 5mg/ml; BioXCell). Cells were either treated with full RPMI for Th0 conditions or with RPMI containing optimal Th17 conditions [IL-1β (40 ng/ml), IL-6 (100 ng/ml), IL-23 (20 ng/ml), and TGF- β (10 ng/ml); with or without CCL2 (5 ng/ml)] or Th1 [IL-12 (10 ng/ml)] for 3 days. Experiments were also performed in suboptimal Th17 conditions [5 ng/ml TGF-β (5 ng/ml) and IL-6 (20 ng/ml) with or without CCL2 (5 ng/ml)]. Cytokines were from R&D Systems.

Flow cytometry

CNS tissue homogenates were incubated in digestion medium containing 0.5 mg/ml Collagenase Type I (Worthington Biochemical) and 1,000 U/ml DNase I (Sigma-Aldrich) for 45 min, following myelin debris removal using a Percoll gradient. LNs were incubated in digestion medium RPMI supplemented with 0.1 mg/ml DNase I (Invitrogen), and 0.1mg/ml liberase (Roche). Collected single-cell suspensions were filtered. Resulting cell suspensions were incubated with following antibodies: anti-CD45 (clone 30-F11, Thermo Fisher Scientific), anti-Ly6G (clone 1A8, Biolegend), anti-Ly6C (clone HK1.4, Biolegend). Dead cells were excluded using Ghost Dye (eBioscience). For cytokine analysis, LN were cultured in complete medium (RPMI media containing 10% FCS, supplemented with L-glutamine and antibiotics) with 50 ng/ml PMA and 500 ng/ml ionomycin (Sigma-Aldrich) in the presence of Golgiplug (BD Biosciences) for 4 h, followed by FACS staining. Cells were stained with Ghost Dye, CD4 (clone GK1.5, Biolegend), IL-17 (Clone TC11-18H10.1, Biolegend), IL-10 (JES5-16E3, Biolegend) and IFNγ (XMG1.2, Biolegend). To assess T cell differentiation, in vitro differentiated $CD4^+$ T cells were stained with

Ghost Dye, CD4 (clone GK1.5, Biolegend) and IL-17 (Clone TC11-18H10.1, Biolegend). Samples were acquired with BD LSR Fortessa and analyzed using FlowJo software (TreeStar).

Immune cell isolation

LNs from naïve mice were incubated in digestion medium RPMI supplemented with 0.1 mg/ml DNase I (Invitrogen), and 0.1mg/ml liberase (Roche). Single cell suspensions were incubated with CD45 and anti-Ter-119 microbeads (Miltenyi Biotech). After selection (MACS column, Miltenyi Biotech), $CD45^-$ and $CD45^+$ populations were plated overnight in complete RPMI. Cells were stimulated with IL-17 (200 ng/ml) for 24 hours.

Immunoblotting and ELISA

Immunoblotting Abs: mouse IMP2 (MBL, 1:1000; RN008P); Human IMP2 (Cell Signaling, 1:1000; 14672), YY1 (Santa Cruz Biotechnology, 1:1000; sc-1703), β-actin (Abcam, 1:25,000; ab49900). Western blots developed with a FluorChem E imager (Protein Simple, Santa Clara CA). CCL2, IL-17 and IFNγ ELISA kits were used per manufacturer's instructions (R&D Systems).

Data and Code Availability

Imp2$^{-/-}$ mice are available by MTA from Oxford University. *Il17ra*$^{-/-}$ mice are under MTA from Amgen. All other mice are commercially available. RNA-seq data is available through the NCBI GEO resource under accession number GSE180561.

Statistics

One-way ANOVA with post hoc Tukey's analysis or Mann-Whitney test or Student's *t*-test were used to assess statistical significance, with $P < 0.05$ considered significant. Data were analyzed on Graphpad Prism. Each symbol represents one mouse unless indicated. *P<0.05, **<0.01, ***<0.001, ****<0.0001. P values less than 0.05 were considered significant.

Study approval.

All the experiments were conducted following NIH guidelines under protocols approved by the University of Pittsburgh IACUC (Protocol # 20037105).

Author Contributions

Conceptualization: RB, NA, SLG, MJM; Methodology, RB, NA, CZ, QL, SM; Investigation: RB, NA, CZ, QL, SM; Writing – original draft, RB, SLG; writing- review and editing, NA, MJM, CZ, QL; Funding Acquisition, SLG, MJM; Supervision, SLG, MJM.

Acknowledgments

NIH grants supported SLG (AI147383) and MJM (AI148356). We thank Drs. Liliana Minichiello (Oxford University, Oxford, United Kingdom), Joseph Avruch and Ning Dai (Harvard University, Boston, MA) for providing *Imp2*$^{-/-}$ mice and helpful comments. We are grateful to Amgen for *Il17ra*$^{-/-}$ mice. We thank Bianca Coleman for assistance with mouse breeding.

References

1. Ransohoff RM. Animal models of multiple sclerosis: the good, the bad and the bottom line. *Nat Neurosci.* 2012;15(8):1074-7.
2. Karpus WJ, Lukacs NW, et al. Differential CC chemokine-induced enhancement of T helper cell cytokine production. *J Immunol.* 1997;158(9):4129-36.
3. Kennedy KJ, Strieter RM, et al. Acute and relapsing experimental autoimmune encephalomyelitis are regulated by differential expression of the CC chemokines macrophage inflammatory protein-1alpha and monocyte chemotactic protein-1. *J Neuroimmunol.* 1998;92(1-2):98-108.
4. Fife BT, Huffnagle GB, et al. CC chemokine receptor 2 is critical for induction of experimental autoimmune encephalomyelitis. *The Journal of experimental medicine.* 2000;192(6):899-905.
5. Izikson L, Klein RS, et al. Resistance to experimental autoimmune encephalomyelitis in mice lacking the CC chemokine receptor (CCR)2. *J Exp Med.* 2000;192(7):1075-80.
6. Huang DR, Wang J, et al. Absence of monocyte chemoattractant protein 1 in mice leads to decreased local macrophage recruitment and antigen-specific T helper cell type 1 immune response in experimental autoimmune encephalomyelitis. *J Exp Med.* 2001;193(6):713-26.
7. Kara EE, McKenzie DR, et al. CCR2 defines in vivo development and homing of IL-23-driven GM-CSF-producing Th17 cells. *Nat Commun.* 2015;6:8644.
8. Bakos E, Thaiss CA, et al. CCR2 Regulates the Immune Response by Modulating the Interconversion and Function of Effector and Regulatory T Cells. *J Immunol.* 2017;198(12):4659-71.
9. Dasoveanu DC, Park HJ, et al. Lymph node stromal CCL2 limits antibody responses. *Sci Immunol.* 2020;5(45).
10. Martin EW, Pacholewska A, et al. Integrative analysis suggests cell type-specific decoding of NF-kappaB dynamics. *Sci Signal.* 2020;13(620).
11. Wojkowska DW, Szpakowski P, et al. Interleukin 17A Promotes Lymphocytes Adhesion and Induces CCL2 and CXCL1 Release from Brain Endothelial Cells. *Int J Mol Sci.* 2017;18(5).
12. Kebir H, Kreymborg K, et al. Human TH17 lymphocytes promote blood-brain barrier disruption and central nervous system inflammation. *Nat Med.* 2007;13(10):1173-5.
13. Li X, Bechara R, et al. Interleukin 17 receptor-based signaling and implications for disease. *Nat Immunol.* 2019;20:1594-602.
14. Hildebrand DG, Alexander E, et al. IkappaBzeta is a transcriptional key regulator of CCL2/MCP-1. *J Immunol.* 2013;190(9):4812-20.
15. Carpenter S, Ricci EP, et al. Post-transcriptional regulation of gene expression in innate immunity. *Nat Rev Immunol.* 2014;14(6):361-76.
16. Degrauwe N, Suva ML, et al. IMPs: an RNA-binding protein family that provides a link between stem cell maintenance in normal development and cancer. *Genes Dev.* 2016;30(22):2459-74.
17. Dai N. The Diverse Functions of IMP2/IGF2BP2 in Metabolism. *Trends Endocrinol Metab.* 2020;31(9):670-9.

18. Bechara R, Amatya N, et al. The m(6)A reader IMP2 directs autoimmune inflammation through an IL-17- and TNFalpha-dependent C/EBP transcription factor axis. *Sci Immunol.* 2021;6(61).
19. McGeachy MJ, Cua DJ, et al. The IL-17 Family of Cytokines in Health and Disease. *Immunity.* 2019;50(4):892-906.
20. Majumder S, Amatya N, et al. IL-17 metabolically reprograms activated fibroblastic reticular cells for proliferation and survival. *Nature immunology.* 2019;20:534-45.
21. Majumder S, and McGeachy MJ. IL-17 in the Pathogenesis of Disease: Good Intentions Gone Awry. *Annual review of immunology.* 2021;39:537-56.
22. Dai N, Zhao L, et al. IGF2BP2/IMP2-Deficient mice resist obesity through enhanced translation of Ucp1 mRNA and Other mRNAs encoding mitochondrial proteins. *Cell Metab.* 2015;21(4):609-21.
23. Conway AE, Van Nostrand EL, et al. Enhanced CLIP Uncovers IMP Protein-RNA Targets in Human Pluripotent Stem Cells Important for Cell Adhesion and Survival. *Cell Rep.* 2016;15(3):666-79.
24. Degrauwe N, Schlumpf TB, et al. The RNA Binding Protein IMP2 Preserves Glioblastoma Stem Cells by Preventing let-7 Target Gene Silencing. *Cell Rep.* 2016;15(8):1634-47.
25. Henness S, Johnson CK, et al. IL-17A augments TNF-alpha-induced IL-6 expression in airway smooth muscle by enhancing mRNA stability. *J Allergy Clin Immunol.* 2004;114(4):958-64.
26. Amatya N, EE C, et al. IL-17 integrates multiple self-reinforcing, feed-forward mechanisms through the RNA-binding protein Arid5a. *Science Signaling.* 2018;11:eaat4617.
27. Masuda K, Ripley B, et al. Arid5a controls IL-6 mRNA stability, which contributes to elevation of IL-6 level in vivo. *Proc Natl Acad Sci U S A.* 2013.
28. Huang H, Weng H, et al. Recognition of RNA N(6)-methyladenosine by IGF2BP proteins enhances mRNA stability and translation. *Nat Cell Biol.* 2018;20(3):285-95.
29. Bechara R, and Gaffen SL. '(m(6))A' stands for 'autoimmunity': reading, writing, and erasing RNA modifications during inflammation. *Trends Immunol.* 2021;42(12):1073-6.
30. Herjan T, Yao P, et al. HuR is required for IL-17-induced Act1-mediated CXCL1 and CXCL5 mRNA stabilization. *J Immunol.* 2013;191(2):640-9.
31. Hafner M, Landthaler M, et al. Transcriptome-wide identification of RNA-binding protein and microRNA target sites by PAR-CLIP. *Cell.* 2010;141(1):129-41.
32. Fan J, Ishmael FT, et al. Chemokine transcripts as targets of the RNA-binding protein HuR in human airway epithelium. *J Immunol.* 2011;186(4):2482-94.
33. Gschwandtner M, Derler R, et al. More Than Just Attractive: How CCL2 Influences Myeloid Cell Behavior Beyond Chemotaxis. *Front Immunol.* 2019;10:2759.
34. Kafasla P, Skliris A, et al. Post-transcriptional coordination of immunological responses by RNA-binding proteins. *Nature immunology.* 2014;15(6):492-502.
35. Panganiban RP, Vonakis BM, et al. Coordinated post-transcriptional regulation of the chemokine system: messages from CCL2. *J Interferon Cytokine Res.* 2014;34(4):255-66.
36. Herjan T, Yao P, et al. HuR is required for IL-17-induced Act1-mediated CXCL1 and CXCL5 mRNA stabilization. *J Immunol.* 2013;191(2):640-9.
37. Chen J, Cascio J, et al. Posttranscriptional gene regulation of IL-17 by the RNA-binding protein HuR is required for initiation of experimental autoimmune encephalomyelitis. *J Immunol.* 2013;191(11):5441-50.

38. Herjan T, Hong L, et al. IL-17-receptor-associated adaptor Act1 directly stabilizes mRNAs to mediate IL-17 inflammatory signaling. *Nat Immunol.* 2018;19(4):354-65.
39. Dai N, Rapley J, et al. mTOR phosphorylates IMP2 to promote IGF2 mRNA translation by internal ribosomal entry. *Genes Dev.* 2011;25(11):1159-72.
40. Chesik D, De Keyser J, et al. Insulin-like growth factor binding proteins: regulation in chronic active plaques in multiple sclerosis and functional analysis of glial cells. *Eur J Neurosci.* 2006;24(6):1645-52.
41. Lanzillo R, Di Somma C, et al. Insulin-like growth factor (IGF)-I and IGF-binding protein-3 serum levels in relapsing-remitting and secondary progressive multiple sclerosis patients. *Eur J Neurol.* 2011;18(12):1402-6.
42. DiToro D, Harbour SN, et al. Insulin-Like Growth Factors Are Key Regulators of T Helper 17 Regulatory T Cell Balance in Autoimmunity. *Immunity.* 2020;52(4):650-67 e10.
43. Du L, Lin L, et al. IGF-2 Preprograms Maturing Macrophages to Acquire Oxidative Phosphorylation-Dependent Anti-inflammatory Properties. *Cell Metab.* 2019;29(6):1363-75 e8.
44. Screpanti I, Romani L, et al. Lymphoproliferative disorder and imbalanced T-helper response in C/EBP beta-deficient mice. *EMBO J.* 1995;14(9):1932-41.
45. Zhou Y, Zeng P, et al. SRAMP: prediction of mammalian N6-methyladenosine (m6A) sites based on sequence-derived features. *Nucleic Acids Res.* 2016;44(10):e91.
46. Xuan JJ, Sun WJ, et al. RMBase v2.0: deciphering the map of RNA modifications from epitranscriptome sequencing data. *Nucleic Acids Res.* 2018;46(D1):D327-D34.
47. Xiao P, Li M, et al. TTP protects against acute liver failure by regulating CCL2 and CCL5 through m6A RNA methylation. *JCI Insight.* 2021;6(23).
48. Preitner N, Quan J, et al. IMP2 axonal localization, RNA interactome, and function in the development of axon trajectories. *Development.* 2016;143(15):2753-9.
49. Zhu X, Yan J, et al. RBM3 promotes neurogenesis in a niche-dependent manner via IMP2-IGF2 signaling pathway after hypoxic-ischemic brain injury. *Nat Commun.* 2019;10(1):3983.
50. Fujii Y, Kishi Y, et al. IMP2 regulates differentiation potentials of mouse neocortical neural precursor cells. *Genes Cells.* 2013;18(2):79-89.
51. Krishnamurty AT, and Turley SJ. Lymph node stromal cells: cartographers of the immune system. *Nature immunology.* 2020;21(4):369-80.
52. Buechler MB, and Turley SJ. A short field guide to fibroblast function in immunity. *Semin Immunol.* 2018;35:48-58.
53. Nygaard G, and Firestein GS. Restoring synovial homeostasis in rheumatoid arthritis by targeting fibroblast-like synoviocytes. *Nat Rev Rheumatol.* 2020;16(6):316-33.
54. Spallanzani RG, Zemmour D, et al. Distinct immunocyte-promoting and adipocyte-generating stromal components coordinate adipose tissue immune and metabolic tenors. *Sci Immunol.* 2019;4(35).
55. Kohlgruber A, Gal-Oz S, et al. Gammadelta T cells producing interleukin-17A regulate adipose regulatory T cell homeostasis and thermogenesis. *Nature immunology.* 2018;19:464-74.
56. Havrdova E, Belova A, et al. Activity of secukinumab, an anti-IL-17A antibody, on brain lesions in RRMS: results from a randomized, proof-of-concept study. *J Neurol.* 2016;263(7):1287-95.

57. Volpe E, Battistini L, et al. Advances in T Helper 17 Cell Biology: Pathogenic Role and Potential Therapy in Multiple Sclerosis. *Mediators of inflammation.* 2015;2015:475158.
58. Lovett-Racke AE, Yang Y, et al. Th1 versus Th17: are T cell cytokines relevant in multiple sclerosis? *Biochim Biophys Acta.* 2011;1812(2):246-51.
59. Wang F, Zuroske T, et al. RNA therapeutics on the rise. *Nat Rev Drug Discov.* 2020;19(7):441-2.

FIGURES AND LEGENDS

Figure 1

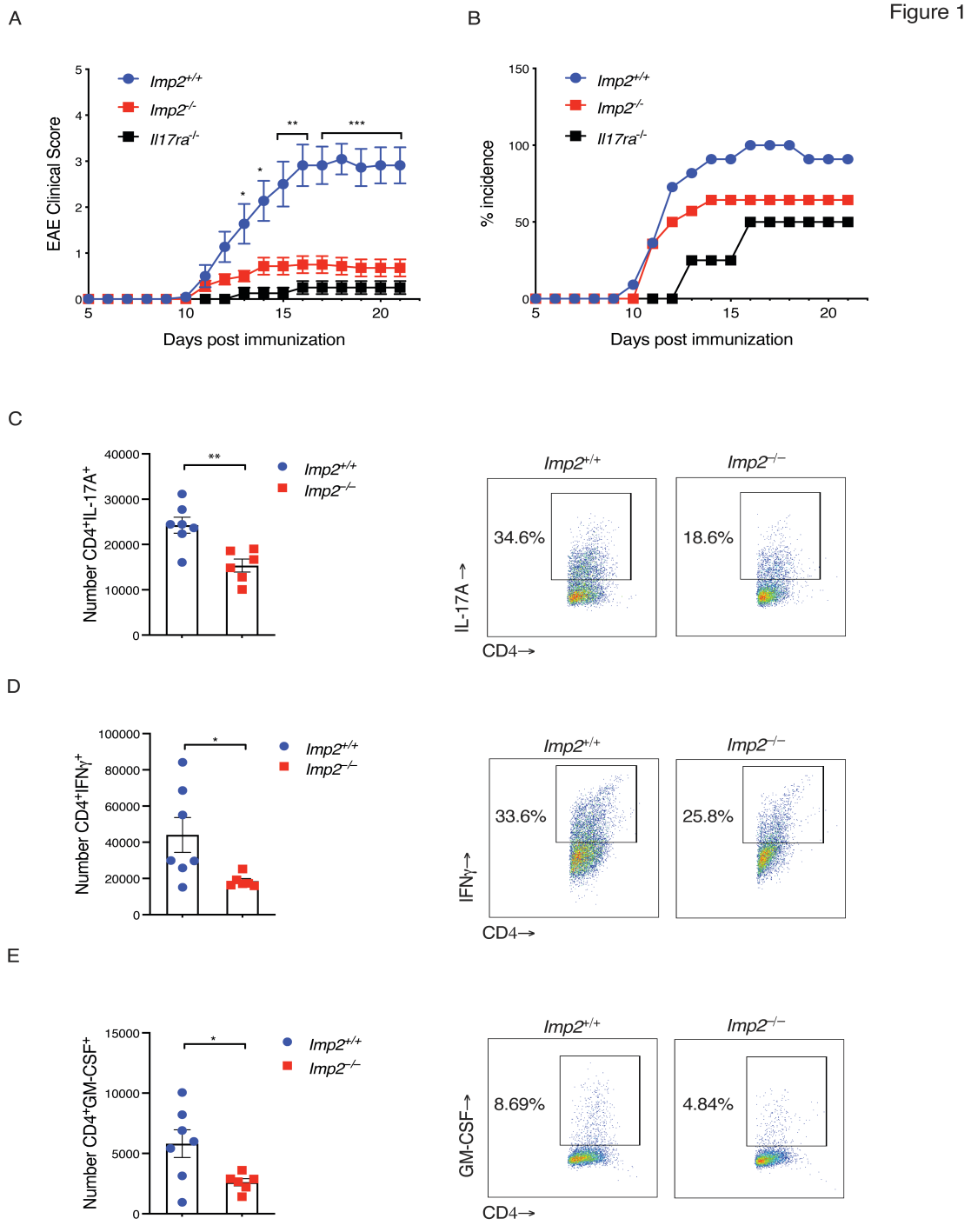

Fig 1. IMP2$^{-/-}$ mice are refractory to IL-17-driven neuroinflammation

(A) The indicated mice (*Imp2*$^{+/+}$ n=11; *Imp2*$^{-/-}$ n=14 and *Il17ra*$^{-/-}$ n=4) were subjected to EAE and

clinical scores assessed daily. Mean clinical scores pooled from 3 independent experiments are shown. (B) Percentage of mice exhibiting EAE symptoms (incidence). (C-E) The indicated mice were subjected to EAE (*Imp2*$^{+/+}$ n=7; *Imp2*$^{-/-}$ n=6). CNS cells harvested on day 16 were treated with PMA/ionomycin for 4 h. Cells were stained for CD4, IL-17A, GM-CSF and IFNγ, and quantified by flow cytometry. *Right*: Representative FACS plots. Data were pooled from 2 independent experiments. Throughout, each symbol represents one mouse. *P<0.05, **P<0.01 by *P<0.05, **P<0.01, ***P<0.001, by Mann-Whitney test (A), unpaired Student t-test (C-E).

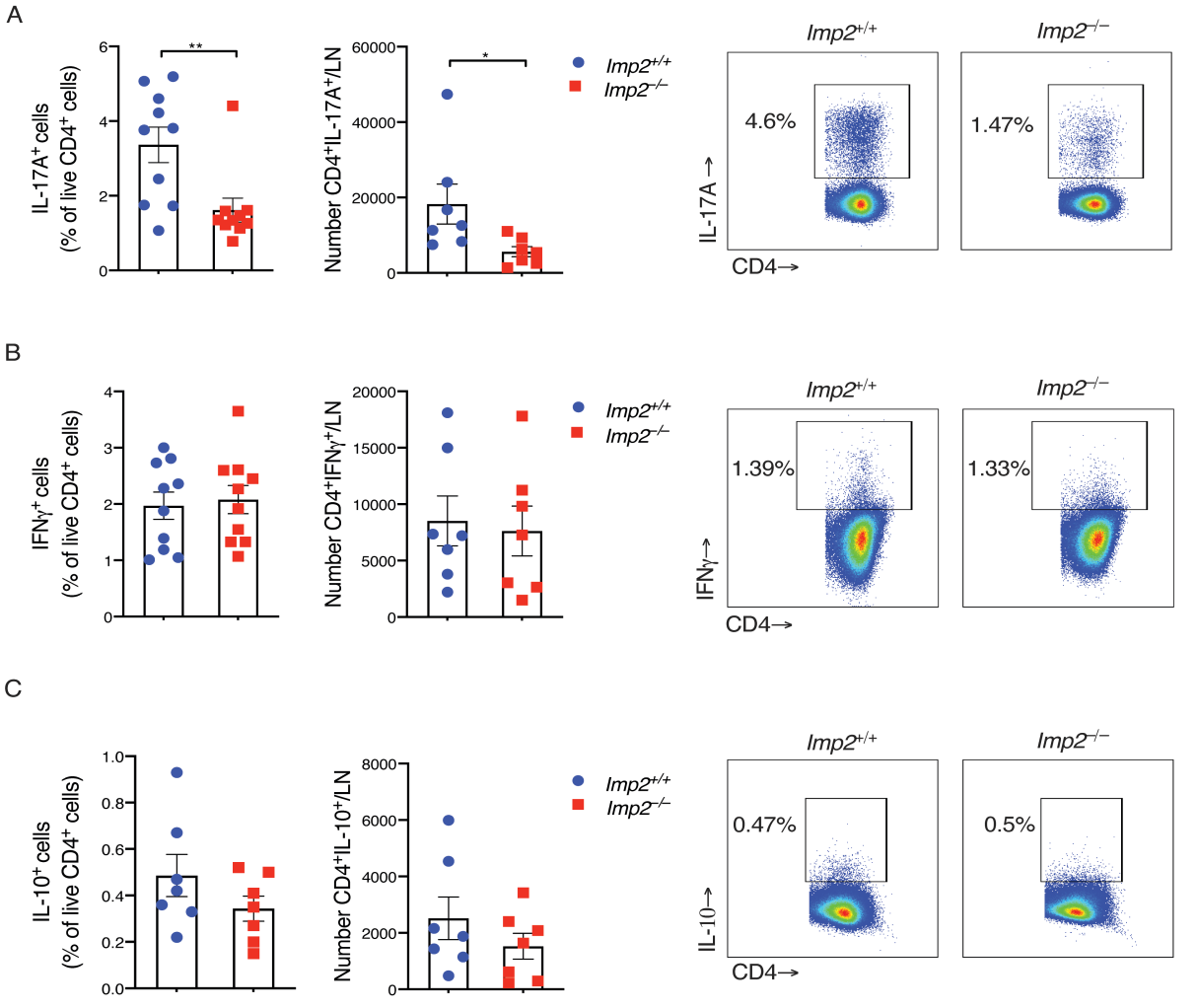

Fig 2. IMP2 promotes Th17 cell generation

(A-C) *Imp2*$^{+/+}$ (n=7-10) and *Imp2*$^{-/-}$ (n=7-10) mice were subjected to EAE. Inguinal Lymph nodes cells harvested on day 10 were treated with PMA/ionomycin for 4 h. Cells were stained for CD4, IL-17A, IL-10 and IFNγ, and quantified by flow cytometry. Data were pooled from 2-3 independent experiments. *Right*: Representative FACS plots. Throughout, each symbol represents one mouse. *P<0.05, **P<0.01 by unpaired Student t-test.

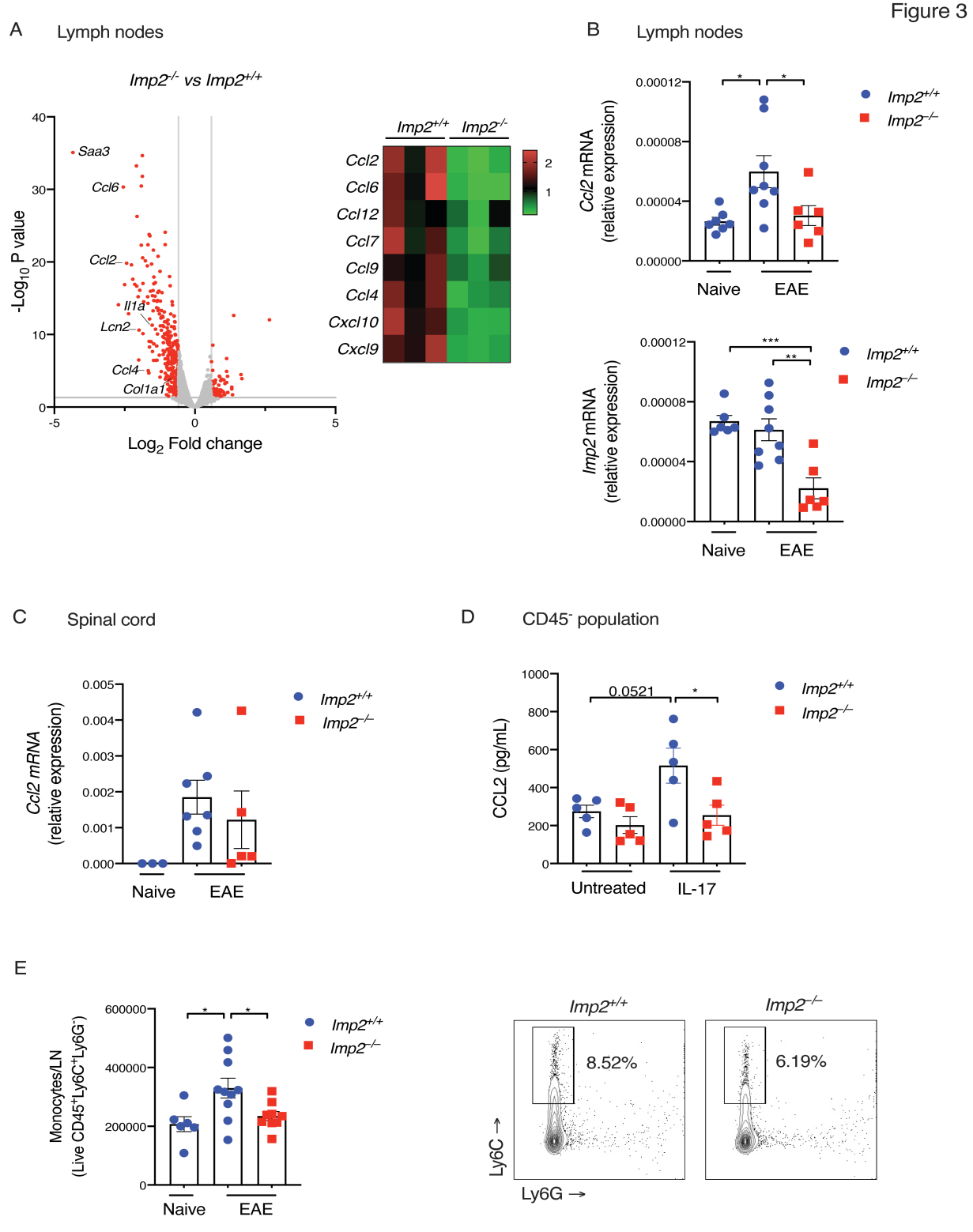

Fig 3. IMP2 promotes Ccl2 expression and monocyte recruitment in LN

(A-B) *Imp2*$^{+/+}$ and *Imp2*$^{-/-}$ mice were subjected to EAE. Inguinal LN homogenates were prepared

on day 7 post-EAE. (A) RNA-seq (*Imp2*$^{+/+}$ n = 3 and *Imp2*$^{-/-}$ n = 3) was performed on the Illumina platform. Volcano plots showing the genes that were significantly changed (P value < 0.05, fold change of >1.5 or <−1.5 and RPKM in *Imp2*$^{+/+}$ >1). Transcripts that are known to be IL-17-regulated are annotated. *Right*; Heat map of chemokines that are differentially regulated based on IPA. (B) *Imp2*$^{+/+}$ n=8; *Imp2*$^{-/-}$ n=6 were subjected to EAE. Indicated mRNAs were assessed by qPCR in inguinal LNs at day 7. Data show relative expression ± SEM from 2 independent experiments. (C) The indicated mice (*Imp2*$^{+/+}$ n=6; *Imp2*$^{-/-}$ n=6) were subjected to EAE, and RNA from spinal cord day 15 was subjected to qPCR normalized to *Gapdh*. Data show relative expression ± SEM from 2 independent experiments. (D) CD45^{-} cells from *Imp2*$^{+/+}$ n=5; *Imp2*$^{-/-}$ n=5 mice were treated with IL-17 for 24 h and conditioned media assessed by ELISA. Data show mean pg/ml ± SEM from 2 independent experiments. (E) *Imp2*$^{+/+}$ n=10; *Imp2*$^{-/-}$ n=9 mice were subjected to EAE. Inguinal LN homogenates were prepared on day 7 post-EAE. Live monocytes were determined by Ly6C and Ly6G staining, gated on the live CD45^{+} population. *Left:* Numbers of live CD45^{+} Ly6C^{+}Ly6G^{-} cells, pooled from 3 independent experiments. *Right*; Representative FACS plots. Throughout, each symbol represents one mouse. *P<0.05, **P<0.01, ***P<0.001, by ANOVA with post-hoc Tukey test (C-E).

Figure 4

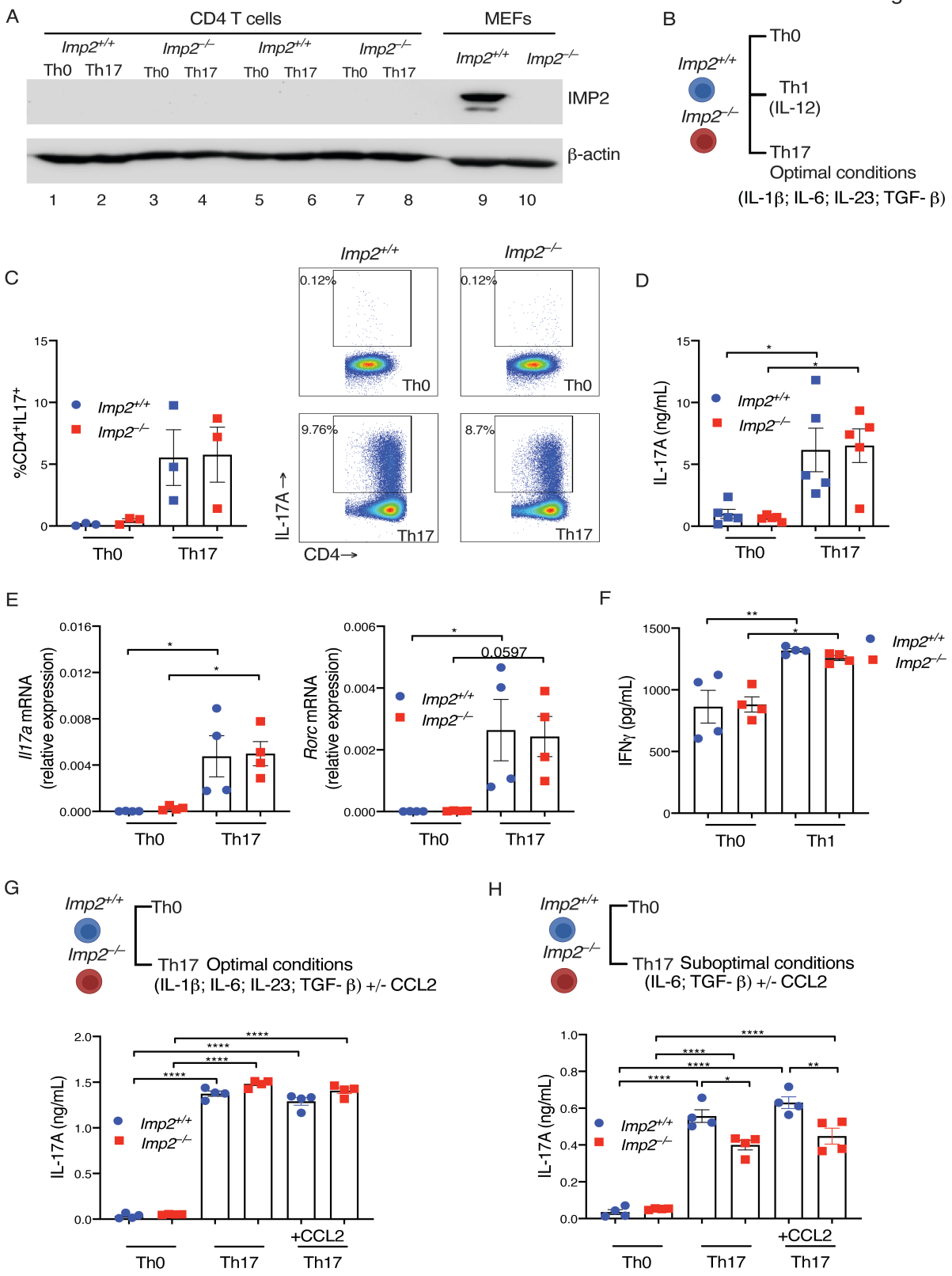
A
CD4 T cells
MEFs
Imp2+/+
Imp2−/−
Th0
Th17
IMP2
β-actin
1 2 3 4 5 6 7 8 9 10
B
Th0
Th1
(IL-12)
Th17
Optimal conditions
(IL-1β; IL-6; IL-23; TGF- β)
C
%CD4+IL17+
0.12%
9.76%
8.7%
IL-17A →
CD4→
D
IL-17A (ng/mL)
E
Il17a mRNA (relative expression)
Rorc mRNA (relative expression)
0.0597
F
IFNγ (pg/mL)
G
Th17 Optimal conditions
(IL-1β; IL-6; IL-23; TGF- β) +/- CCL2
H
Th17 Suboptimal conditions
(IL-6; TGF- β) +/- CCL2
+CCL2

Fig 4. Th1 and Th17-extrinsic activities of IMP2

(A) IMP2 expression by WB on whole cell lysates from $CD4^+$ T cells cultured in Th0 conditions (Lanes 1, 3, 5, 7), Th17 conditions (IL-6, IL-23, TGFβ and IL-1β) (Lanes 2, 4, 6, 8). Control lysates from *Imp2*$^{+/+}$ and *Imp2*$^{-/-}$ MEFs (Lanes 9-10). (B) Diagram of in vitro $CD4^+$ T cell polarization conditions. (C-E) $CD4^+$ T cells were isolated from spleen and stimulated for 3 d with plate-bound anti-CD3 and anti-CD28 under Th0 or optimal Th17 conditions (IL-6, IL-23, TGFβ and IL-1β) for 3 days. (C) Cells were stimulated with PMA/ionomycin for 4 h, stained for CD4 and IL-17, and quantified by flow cytometry. *Right*: Representative FACS plots from 3 independent experiments. (D) ELISA was performed on supernatants collected after 3 days treatment with anti-CD3 and anti-CD28. Data were pooled from 2 independent experiments (E) qPCR of the indicated mRNAs in T cells after 3 days of anti-CD3 and anti-CD28. Data show fold-change mean ± SEM from 2 independent experiments. (F) $CD4^+$ T cells were isolated from spleen and stimulated for 3 d with plate-bound anti-CD3 and anti-CD28 under Th0 or Th1 conditions (IL-12). ELISA was performed on supernatants collected after 3 d anti-CD3 plus anti-CD28. (G-H) $CD4^+$ T cells were isolated from spleen and stimulated for 3 d with plate-bound anti-CD3 and anti-CD28 under Th0 or optimal Th17 conditions (G) (IL-6, IL-23, TGFβ and IL-1β) or suboptimal Th17 conditions (H) (IL-6 and TGFβ) +/- CCL2 for 3 d. ELISA was performed on supernatants collected after 3 d anti-CD3 plus anti-CD28. Each symbol represents one mouse. *P<0.05; **P<0.01; ****P<0.0001 by ANOVA with post-hoc Tukey test.

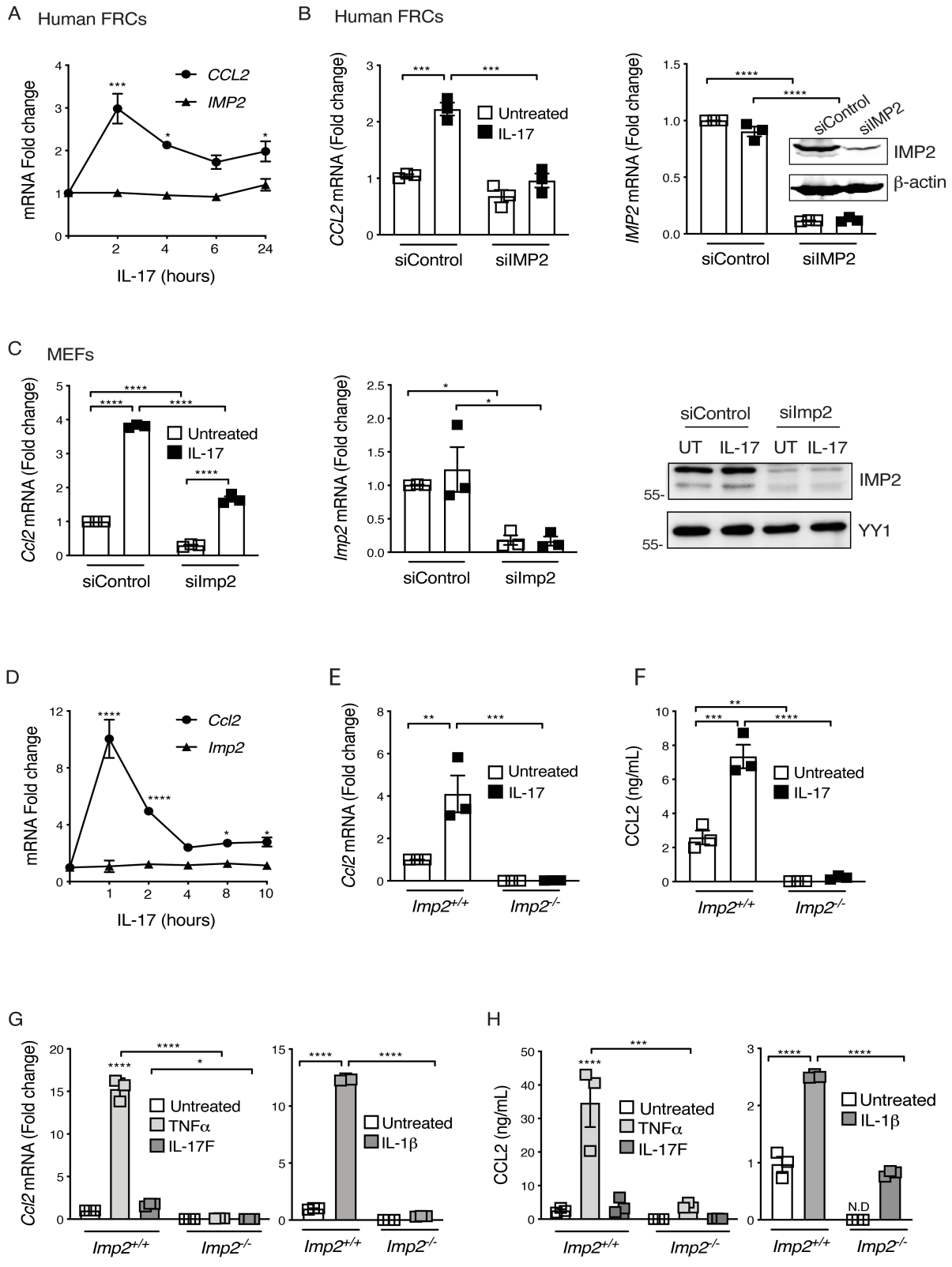
A
Human FRCs
mRNA Fold change
CCL2
IMP2
IL-17 (hours)
B
Human FRCs
CCL2 mRNA (Fold change)
Untreated
IL-17
siControl
siIMP2
IMP2 mRNA (Fold change)
siControl
siIMP2
IMP2
β-actin
C
MEFs
Ccl2 mRNA (Fold change)
Untreated
IL-17
siControl
siImp2
Imp2 mRNA (Fold change)
siControl
siImp2
siControl
siImp2
UT
IL-17
UT
IL-17
55-
IMP2
55-
YY1
D
mRNA Fold change
Ccl2
Imp2
IL-17 (hours)
E
Ccl2 mRNA (Fold change)
Untreated
IL-17
Imp2+/+
Imp2-/-
F
CCL2 (ng/mL)
Untreated
IL-17
Imp2+/+
Imp2-/-
G
Ccl2 mRNA (Fold change)
Untreated
TNFα
IL-17F
Imp2+/+
Imp2-/-
Untreated
IL-1β
Imp2+/+
Imp2-/-
H
CCL2 (ng/mL)
Untreated
TNFα
IL-17F
Imp2+/+
Imp2-/-
Untreated
IL-1β
N.D
Imp2+/+
Imp2-/-

Fig 5. IL-17 induces CCL2 via the RNA binding protein IMP2

(A) Human tonsillar FRCs were given human IL-17A for the indicated times and *CCL2* and *IMP2 (IGF2BP2)* assessed by qPCR. Data shown as mean fold change ± SEM from 3 independent experiments. (B) Human FRCs were transfected with siRNAs targeting *IMP2* or scrambled control, treated ± IL-17A for 2 h and *CCL2* assessed by qPCR. Data are normalized to untreated samples with control siRNA, from 3 independent experiments ± SEM. *Inset;* IMP2 expression assessed by WB in human FRCs, representative of 2 independent experiments. (C) Primary MEFs were transfected with siRNAs targeting *Imp2* or control and treated ± IL-17A for 8 h. *Left:* Indicated mRNAs were assessed by qPCR. Data are normalized to untreated samples transfected with control siRNA from 3 independent experiments ± SEM. *Right*: IMP2 levels assessed by WB in MEFs. (D) MEFs were treated with IL-17A and *Ccl2* and *Imp2* were assessed by qPCR normalized to *Gapdh*. Data shown as mean fold change ± SEM from 3 independent experiments. (E) $Imp2^{+/+}$ or $Imp2^{-/-}$ MEFs were treated ± IL-17A for 8 h and *Ccl2* assessed by qPCR. Data shown as mean fold change ± SEM from 3 independent experiments. (F) $Imp2^{+/+}$ or $Imp2^{-/-}$ cells were treated with IL-17A for 24 h and CCL2 in conditioned supernatants was assessed by ELISA. Data show ng/ml ± SEM from 3 independent experiments. (G) $Imp2^{+/+}$ or $Imp2^{-/-}$ MEFs were treated ± IL-17F, TNFα, IL-1β for 8 h and *Ccl2* assessed by qPCR. Data shown as mean fold change ± SEM from 3 independent experiments. (H) $Imp2^{+/+}$ or $Imp2^{-/-}$ cells were treated ± IL-17F, TNFα, IL-1β for 24 h and CCL2 in conditioned supernatants was assessed by ELISA. Data shown as ng/ml ± SEM from 3 independent experiments. *P<0.05, **P<0.01, ***P<0.001, ****P<0.0001 by ANOVA with post hoc Tukey's test.

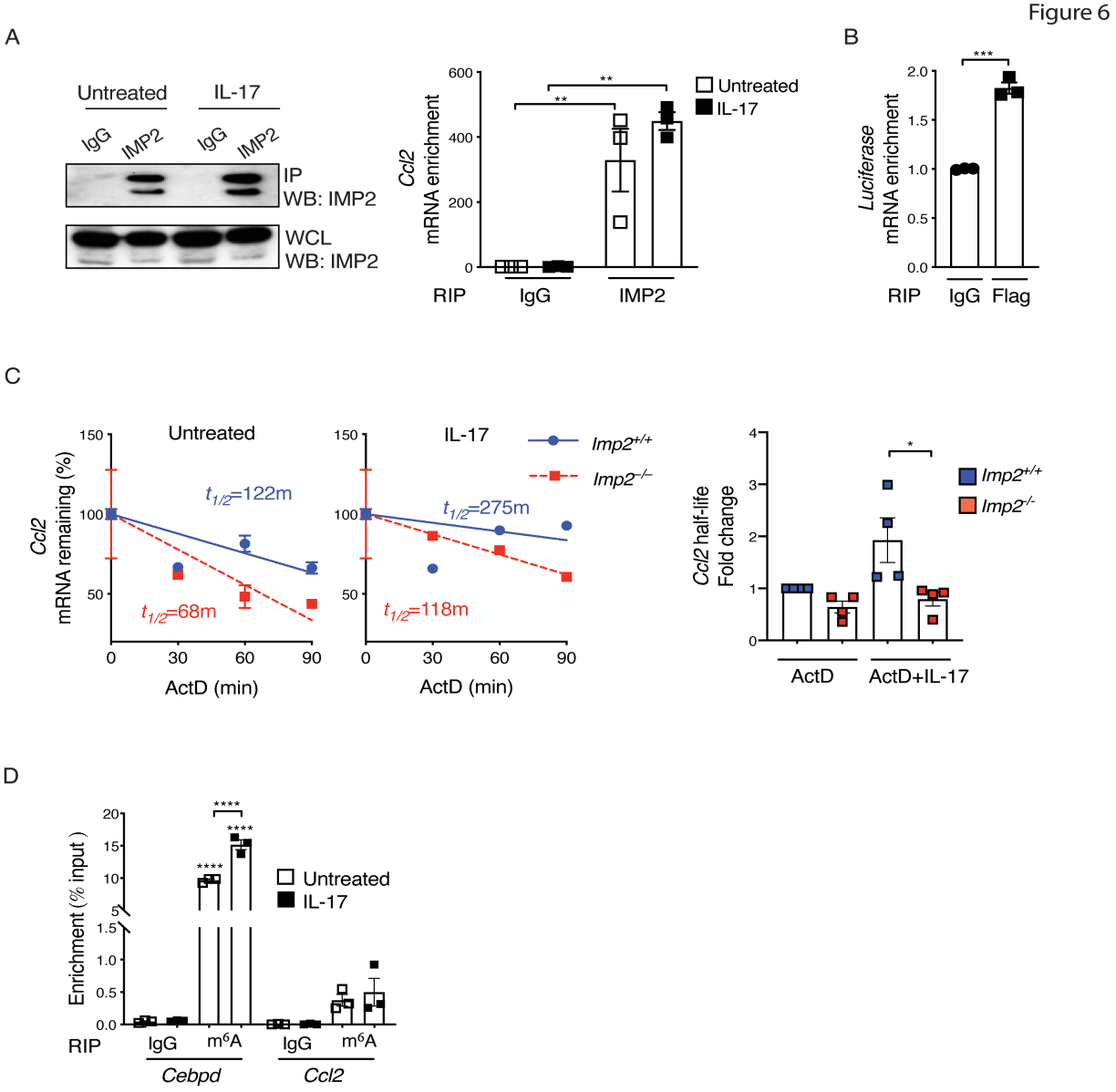

Fig 6. IMP2 binds to Ccl2 mRNA and promotes transcript stability

(A) *Imp2*$^{+/+}$ MEFs were treated ± IL-17 for 3 h and subjected to RIP with anti-IMP2 or IgG control Abs. *Left;* IgG and IMP2 immunoprecipitates from *Imp2*$^{+/+}$ MEFs, assessed by WB. *Right: Ccl2* was assessed by qPCR and normalized to input. Data show mean ± SEM of 3 independent experiments. (B) HEK293T cells were cotransfected with IMP2-FLAG, and a Luc reporter fused to WT *Ccl2*-3′UTR. Lysates were subjected to RIP with anti-FLAG Abs and Luc mRNA assessed

by qPCR. Data are normalized to input and are representative of 2 independent experiments. (C) MEFs were pre-treated with TNFα for 3 h, incubated with actinomycin D ± IL-17 for the indicated times, and *Ccl2* assessed by qPCR. Data normalized to time=0 (designated 100%) and half-life determined by linear regression, as described (26). *Left:* Representative data. *Right:* Pooled data from 4 independent experiments. (D) MEFs were treated ± IL-17 for 3 h and subjected to RIP with m^6A or IgG control Abs. qPCR of the indicated mRNAs is presented as % input. Data are representative of 2 independent experiments. *P<0.05, **P<0.01, ***P<0.001; ****P<0.0001 by ANOVA with post hoc Tukey's test (A, C, D), unpaired Student t-test (B).

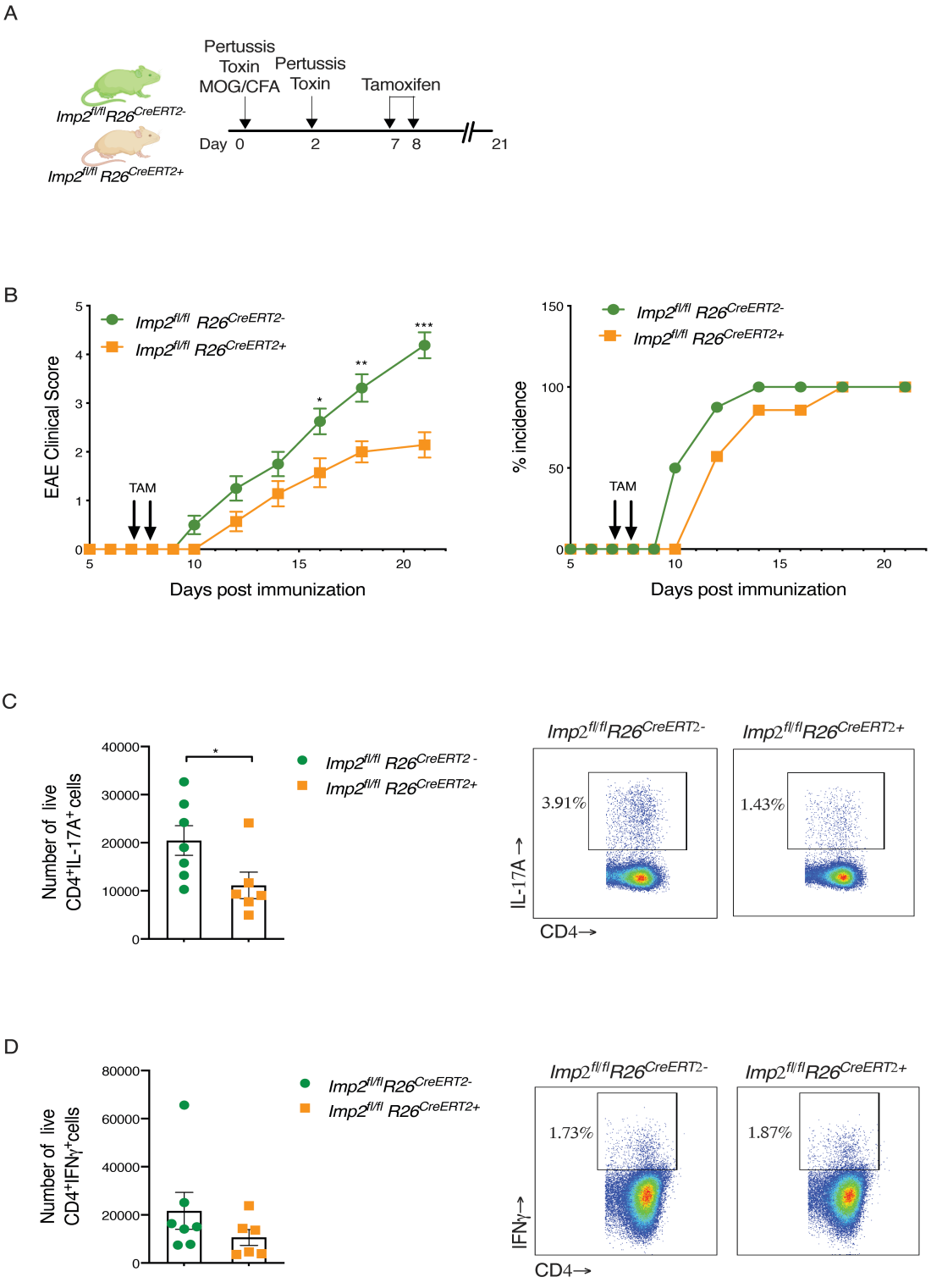

Fig 7. Imp2 deletion post EAE induction decreased EAE.

(A-D) *Imp2*$^{fl/fl}$ and *Imp2*$^{fl/fl}$*R26*^{CreERT2} mice were administered 2 mg tamoxifen (TAM) i.p. for 2 d,

starting day 7 post-EAE. (B) The indicated mice (*Imp2*$^{fl/fl}$*R26*$^{CreERT2-}$ n=8 and *Imp2*$^{fl/fl}$*R26*$^{CreERT+}$ n=7) were subjected to EAE and clinical scores assessed daily. *Left:* Data are presented as mean clinical score, pooled from 2 independent experiments. *Right*: Percentage of mice exhibiting EAE symptoms (incidence). (C-D) *Imp2*$^{fl/fl}$*R26*$^{CreERT2-}$ n=7 and *Imp2*$^{fl/fl}$*R26*$^{CreERT+}$ n=6 mice were subjected to EAE and treated with TAM on day 7 and 8. Lymph nodes were harvested on day 12 and cells treated with PMA/ionomycin for 4 h. Cells were stained for CD4, IL-17A and IFNγ, and quantified by flow cytometry. Data were pooled from 2 independent experiments. *Right*: Representative FACS plots. Each symbol represents one mouse. *P<0.05, **P<0.01, ***P<0.001 by Mann-Whitney test (B) or unpaired Student t-test (C-D).